Development of customized shear layers on smooth and rough surfaces

Phillip M. Ligrani*

Shear layers having different structural properties were produced downstream of devices used to artificially thicken turbulent boundary layers. The means used to produce different structural characteristics are described, along with the effects of changes in structure on wall heat transfer. Results from layers developing over smooth and rough surfaces indicate that alterations of artificial thickening device geometry resulted in larger variations in wall heat transfer near smooth surfaces. The most significant of these occurred when alterations were made of inner boundary layer regions, where mean velocity shows a logarithmic dependence on distance from the wall. Outer region changes in mean velocity and turbulence profiles resulted in less significant changes in wall heat transfer, particularly in the flows over the rough wall.

Keywords: *shear layers, boundary layers, turbulence, surface roughness, heat transfer*

Introduction

Turbulence management is currently employed to achieve a variety of engineering objectives: drag reduction, heat transfer aumentation, heat transfer reduction, heat transfer augmentation, heat transfer manipulation of unsteady flows in aerodynamics. In order to design engineering components which accomplish such tasks, adequate laboratory understanding is required of the cause and effect relationship between the component which is changed to manipulate the flow, and the resulting alterations in turbulence structure. The effect of the structural changes on the property to be 'managed' is then also needed.

According to Hunt[1], 'the art of such flow manipulations is a surprisingly neglected area in fluid mechanics research,' especially considering that engineering designers must know 'how to adjust external boundaries or inlet conditions, or perhaps the fluid properties, to achieve the desired flow.' In a comprehensive review article on body-turbulence interaction, Bushnell[2] reaches a similar conclusion. He focuses attention on 'the effects of the body upon the incident turbulence,' and discusses a variety of topics, including turbulence fields which impinge on surfaces, jet impingement, and vortex–body interaction. Also discussed are the interactions of turbulence fields with porous bodies, two-dimensional bluff bodies, slender bodies, and three-dimensional bodies. Devices to artificially thicken turbulent boundary layers are included in the last category, and also reviewed by Hunt and Fernholz[3] and Ligrani *et al*[4]. In another paper, Bushnell[5] discusses flow management for drag reduction.

* Department of Mechanical Engineering, Naval Postgraduate School, Monterey, CA 93943–5000, USA
Received 27 November 1985 and accepted for publication on 20 May 1986

The shear layers initially resulting from such manipulations are generally different from those without manipulation. Like most flows in nature (eg atmospheric boundary layers) and in many man-made engineering systems (eg flows through turbine passages), 'manipulated' shear layers may be three-dimensional without structural similarity as they develop downstream. Three-dimensional forms of the Navier–Stokes equations are often required to represent such flows, and equations for specified geometry, boundary conditions, two dimensionality, and inlet and exit conditions are not necessarily applicable. Because very few experimental data exist, the 'manipulated' shear layers are rarely modelled, and lie at the edge of our understanding of fluid mechanics phenomena.

The purpose of the present paper is to provide new data on management of boundary layer turbulence, the process by which certain turbulence properties are changed in order to alter and control other properties. Specific objectives are (1) to show how different turbulence structural characteristics may be produced in order to customize shear layers for particular applications, and (2) to show how turbulence may be managed in order to alter and control wall heat transfer. The present results also offer a collection of test cases for prediction codes, and provide new insight into the behaviour of three-dimensional boundary layers which change significantly as they develop downstream.

Flow was studied downstream of devices used to artificially thicken turbulent boundary layers (Ligrani and Moffat[6] and Ligrani *et al*[4]), and the information presented was obtained as the thickening devices were developed. The objective of Refs 4 and 6 was to produce two-dimensional flows with properties representative of boundary layers which developed naturally to the same thickness. For the smooth-wall tests given in the present paper, the connection between management, mean

0142–727X/86/040266–12$3.00

velocity profiles and wall heat transfer are considered. For the rough wall studies, attention is focused on the connection between management, Reynolds stress tensor components, mean velocity, and wall heat transfer.

Experimental facilities and measurement techniques

Smooth-wall studies

Tests made in boundary layers developing over smooth surfaces were conducted in the HMT-1 heat transfer tunnel at Stanford, which was first described by Moffat and Kays[7]. The nozzle of the wind tunnel contained suction slots used to remove any boundary layers near the test section inlet. These were followed by a boundary layer trip and the artificial thickening device. For the present study, the temperature along the plates was maintained constant within 0.2°C. At a freestream velocity of 27 m/s the dynamic pressure varied by less than 0.2 mm of water, to give a zero pressure gradient along the length of the test surface. The freestream turbulence level along the test section was measured to be approximately 0.50 per cent.

The heat transfer test surface was 2.44 m long and consisted of 24 plates which could be electrically heated individually. Losses by conduction to the lower side of the test surface, and by radiation, were accounted for in determination of the wall heat flux. Final results are given in terms of Stanton number versus enthalpy thickness Reynolds number. Enthalpy thicknesses were determined from Stanton number measurements using the energy equation for two-dimensional flow fields: $St = d\Delta_2/dx$.

Mean velocities were measured using a boundary layer pitot probe of 0.508 mm outer diameter in conjunction with a micromanometer. No corrections were made for viscous effects near the wall. The probe was mounted on a traversing mechanism with a micrometer for adjustment of probe position relative to the wall. All profile measurements were made on the centreline of the tunnel, except when spanwise uniformity checks of the mean velocity were made.

Values of local skin friction coefficients $C_f/2$ were estimated from measurements of the Reynolds shear stress $-\overline{u'v'}$ near the wall. A 3 mm slanted hot-wire probe of 5 μm platinum-plated tungsten wire was used for this purpose.

Notation

A_f Spire frontal area
C Constant in smooth law of the wall
C_D Drag coefficient based on area $A \equiv 2g_c F_D/\rho_\infty U_\infty{}^2 A$
$C_f/2$ Local skin friction coefficient $\equiv \tau_w g_c/\rho_\infty U_\infty{}^2$
$\overline{C_f}/2$ Averaged skin friction coefficient
C_p Specific heat of fluid
G Clauser shape factor $\equiv$

$$\frac{1}{\int_0^\infty \left(\frac{U-U_\infty}{U_\tau}\right) dy} \int_0^\infty \left(\frac{U-U_\infty}{U_\tau}\right)^2 dy$$

h Barrier height
k_s Equivalent sand grain roughness
L Hydrodynamic starting length upstream of test surface
$\dot{q}_w''$ Wall heat flux
r Radius of spheres comprising test surface
Re_{Δ_2} Enthalpy thickness Reynolds number $\equiv \Delta_2 U_\infty/\nu$
St Stanton number $\equiv \dot{q}_w''/\{\rho_\infty U_\infty C_p(T_w - T_{\infty,0})\}$
T Mean temperature
T_w Wall temperature
T_∞ Static freestream temperature
$T_{\infty,0}$ Total freestream temperature
u Instantaneous longitudinal velocity
u' Longitudinal velocity fluctuation
U Mean longitudinal velocity
U^+ U/U_τ
U_∞ Freestream velocity
U_τ Friction velocity $\equiv U_\infty (C_f/2)^{1/2}$
v Instantaneous velocity normal to surface
v' Normal velocity fluctuation
w Instantaneous transverse velocity
w' Transverse velocity fluctuation
x Longitudinal coordinate
y Coordinate normal to surface, measured from velocity virtual origin $\equiv y' + \Delta y$
y' Coordinate normal to surface, measured from crests of spherical roughness elements
y^+ yU_τ/ν
Δy Distance between the ball crests and the virtual origin of the velocity profiles
z Transverse coordinate
β Spire height
γ Distance between bar and wall
δ Hydrodynamic boundary layer thickness $\equiv U/U_\infty = 0.99$
δ_2 Momentum thickness $\equiv$

$$\int_0^\infty \frac{\rho U}{\rho_\infty U_\infty}\left(1 - \frac{U}{U_\infty}\right) dy$$

Δ_2 Enthalpy thickness $\equiv$

$$\int_0^\infty \frac{\rho U}{\rho_\infty U_\infty}\left(\frac{T - T_\infty}{T_w - T_\infty}\right) dy$$

θ Upstream spire blade angle
κ Karman constant
ν Kinematic viscosity
ξ Unheated starting length
ρ Density
τ Shear stress
τ_w Local wall shear stress
ω Transverse distance between the centrelines of spires

Subscripts

∞ Freestream

Superscripts

$\overline{\ }$ Mean (time-averaged) value

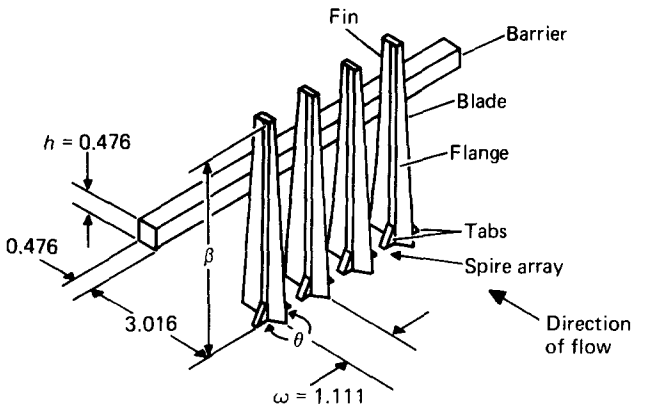

Fig 1 Artificial thickening apparatus for smooth walls from Ref 6, Design C. All dimensions: cm

Rough-wall studies

The wind tunnel used was the HMT-18 roughness rig, first described by Healzer *et al*[8]. The test surface was similar to the one in the smooth-wall facility described above. Each of the 24 test plates consisted of 11 layers of 1.27 mm diameter, oxygen-free, high-conductivity copper spheres packed in the most dense array and brazed together. This uniform spheres roughness had an equivalent sandgrain roughness size of 0.79 mm. The tunnel was a closed-circuit device with a plexiglass top wall, which was flexible for alteration of freestream velocity. For the present tests, the top wall was adjusted to produce a zero-pressure gradient along the test surface to within 0.5 mm of water at a freestream velocity of 27.8 m/s. For all heat transfer measurements, the wall temperature was maintained constant to ± 0.1°C for freestream wall temperature differences of approximately 20°C.

Stanton numbers and enthalpy thicknesses were determined using the same techniques as employed for the layer developing over the smooth wall. Freestream temperatures were measured using an iron–constantan thermocouple probe. All temperature probes were calibrated in a Rosemount Model 910A Temperature Calibration Oil Bath, using a Hewlett-Packard Model 2801A Quartz Thermometer as a standard.

Skin friction coefficients were determined from freestream velocity measurements and from near-wall measurements of the Reynolds shear stress and mean velocity using procedures described in Ref 4. In this approach, the turbulent shear stress term $-\overline{u'v'}/U_\infty^2$ accounts for 96 to 98 percent of the total magnitude of $C_f/2$. The remaining 2 to 4 percent may be considered to be a correction because the shear stress was measured slightly away from the wall.

The mean velocity and six Reynolds stress tensor components were measured using standard hot-wire anemometry techniques. Two types of probes were employed, a DISA 55F04 horizontal wire and a DISA 55F02 slant wire, both mounted on traversing mechanisms similar to the one used for mean velocity profiles near the smooth surface. The sensing length of the horizontal wire was 1.25 mm, the slant wire probe sensing length was slightly longer. The probes were used with TSI Model 1050 bridges operated in constant-temperature/constant-resistance modes with wire overheat ratios of 1.5. The bridges were connected to TSI Model 1052 linearizers, followed either by a Hewlett-Packard Model 2401 C integrating digital voltmeter for mean voltage, or a TSI model 1076 meter for root-mean-square values of the fluctuating voltage. The directional sensitivity of the hot-wire probes was based on Jorgensen's equation[4]. Different rotational positions of the slant-wire probe were used in conjunction with horizontal wire measurements to determine the longitudinal Reynolds stress tensor component $\overline{u'^2}$ and Reynolds stress tensor components $\overline{v'^2}$, $\overline{w'^2}$, $\overline{u'w'}$, $-\overline{u'v'}$ and $\overline{u'w'}$.

Experimental results for smooth wall

The device used to artificially thicken turbulent boundary layers developing over smooth surfaces is shown schematically in Fig 1. It consists of an array of spires and a barrier, each of which extends across the width of the wind tunnel just upstream of the test surface. As the flow approaches the device, a trip 0.025 cm high is encountered on the wall just downstream of the exit plane of the nozzle. The spires are situated 3.0 cm downstream of the trip, and the barrier is situated 3.016 cm downstream of the spires.

Shear layers downstream of Fig 1 device are thicker than would develop naturally without any thickening apparatus. As shown in Fig 2, an extension of the effective length of the wind tunnel test surface is produced, which is denoted L. x_1 is the longitudinal distance measured from the downstream edge of the artificial thickening device, and x_2 is the longitudinal distance measured from the apparent origin of the hydrodynamic flow field[4]. All smooth-wall data were obtained at a freestream velocity of 10.1 m/s.

A summary of smooth-wall test results is given in Table 1. The first step involved adjustment to obtain a spanwise uniform mean flow field. This was also done, as required, after almost every step in the development of the artificially thickened boundary layer. Subsequent flow management schemes are listed chronologically to show how convergence to the flow structure described in Ref 6 was accomplished, where those corresponding to the final design (Fig 1) are denoted by asterisks. Of flows produced by various configurations, the one from the final design has properties most representative of a two-dimensional layer which developed naturally to the same thickness.

Effects of outer region structural adjustments

One way in which outer regions are altered is by changing the shapes of spires. Velocity profiles downstream of three different spire array designs, each followed by a 0.476 cm barrier, are shown in Fig 3.

The velocity profile with the largest differences relative to the freestream velocity is obtained with Design A, which has a blunt trailing edge and no upstream blade. The velocity profile with the smallest differences relative to the freestream velocity is obtained using Design B, which is fully streamlined with upstream and downstream blades. A velocity profile which is between those produced by A and B, and also shows agreement with Simpson *et al*'s[9] data at about the same momentum thickness Reynolds number, is produced by Design C.

Finer adjustments of the velocity profiles than those produced by adding upstream and downstream

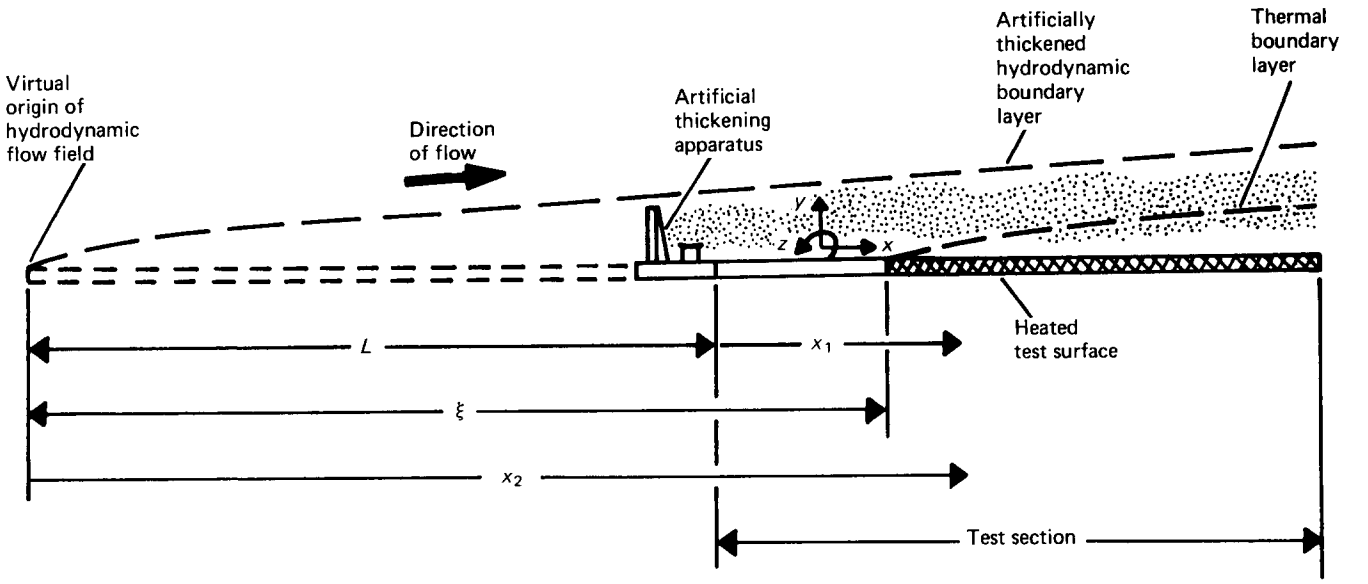

Fig 2 Coordinate system for artificially thickened boundary layers from Ref 4

Table 1 Summary of smooth-wall test results

Development step	Symbols	Design designation	Shear layer alteration	Effects on spatially averaged Stanton numbers
1	◆■	–	Outer region three-dimensionality	Increase with three-dimensionality by 0–3%
2	◑	A without barrier	Existence of region where mean velocity shows logarithmic dependence on distance from wall	Decrease by 0–12%
	◨	A with barrier 0.476 cm high		Nominal
3	◪	A no streamlining	Mean velocity profile shape and magnitude principally in outer region	Decrease by 7–10%
	▼	B fully streamlined		–
	⊙	C Half streamlined[a]		Nominal
		All with barrier 0.476 cm high		
4	○	C with 0.476 cm barrier[a]	Relation between skin friction coefficient and mean velocity in log region	Nominal
	△	C with 0.635 cm barrier		Increase by 10–20%
	□	C with 0.794 cm barrier		Increase by 10–29%

[a] Produces flow representative of a naturally developing, two-dimensional, flat plate turbulent boundary layer on a smooth surface[6]

blades can be made by altering the upstream total angle of each blade, θ (see Fig 1). This is possible since the spanwise momentum flux of fluid diverted between spires is dependent upon direction relative to the freestream, which is a function of θ at the spire upstream edges. The upstream blades also affect turbulent fluctuation intensities, since the intial mechanism for increasing turbulent kinetic energy is mixing between adjacent spires. Also, as spacing between spires increases (larger ω in Fig 1), differences between outer region and freestream velocities are expected to decrease.

The variation of Stanton numbers as outer region structure is changed is shown in Fig 4. Because the effective origin of the hydrodynamic layer is upstream of the thermal layer origin, the boundary layer produced by the artificial thickening device is much thicker than the thermal boundary layers, and Stanton numbers show the effects of an unheated starting length[4]. This is evident from Fig 2, where unheated starting length is denoted ξ. The constant-wall-temperature line is shown on Fig 4 along with a prediction of a boundary layer over a smooth surface with an unheated starting length[10] of 2.60 m. The

unheated starting length curve lies below the one for constant temperature Stanton numbers. Experimental data are initially above the prediction due to some unnatural mixing just downstream of the thickening device. Eventually, measured Stanton numbers for Design C spires with a barrier 0.476 cm high agree with the prediction.

Results in Fig 4 also indicate that Stanton numbers downstream of Design A spires are lower than those downstream of Design C spires. The lower Stanton numbers correspond to lower mean velocities relative to the freestream for $y/\delta < 0.7$–0.8.

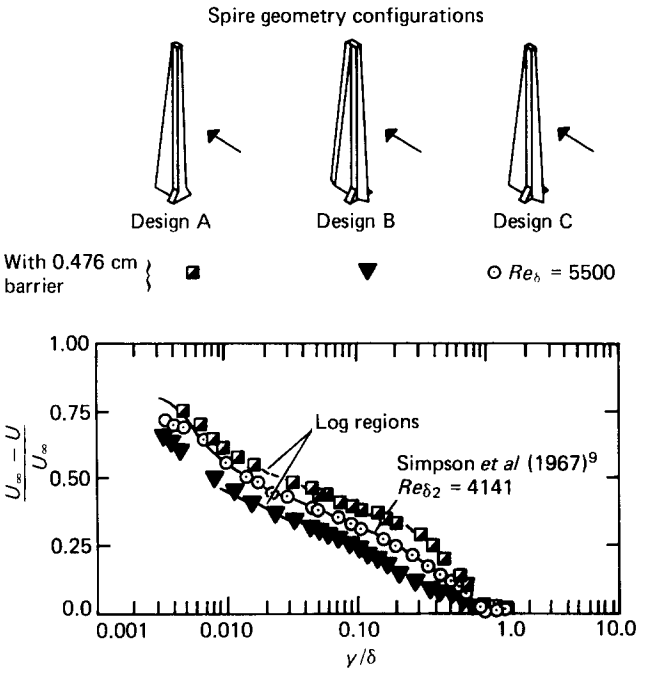

Fig 3 Effects of spire shape changes on mean velocity profiles, $x_1 = 2.08$ m. Symbols given in Table 1

The changes in spire streamlining with Designs A, B, and C result in different magnitudes of form drag on the thickening device, and different values of hydrodynamic starting length L (see Fig 2). An estimate of the dependence of L on geometry can be obtained by equating form drag to the skin friction which would exist for a test section of length L:

$$\frac{\overline{C_f}}{2} L = \frac{C_D}{2} \frac{A_f}{\omega} \tag{1}$$

In Eq (1), C_D is is the drag coefficient for the thickening apparatus based on the frontal area of one spire A_f. If the Schultz–Grunow[11] correlation for $C_f 2$ is then substituted into Eq (1) and the result is rearranged, we have

$$\frac{(0.427)L}{(2.0)\left\{-0.407 + \log\left(\frac{U_\infty L}{\nu}\right)\right\}^{2.64}} = \frac{C_D}{2} \frac{A_f}{\omega} \tag{2}$$

From Eq (2), the hydrodynamic starting length L becomes larger with increasing C_D, A_f and decreasing ω. Increased barrier height h and increased spire height β also result in increased magnitudes of L. In the present study, for the Fig 1 design, $C_D \approx 1.0$. The momentum thickness just downstream of the spires, $\delta_2|_L$ (δ_2 at $x_2 = L$), can be adjusted in the saem way in which the hydrodynamic starting length is changed. This becomes apparaent after substituting for $\overline{C_f/2}$ in Eq (1), using the momentum integral equation to give

$$\delta_2|_L = \frac{C_D}{2} \frac{A_f}{\omega} \tag{3}$$

An indication of the effect of outer region, spanwise mean velocity variations on wall heat transfer is evident from results given in Fig 5. Stanton numbers corresponding to solid diamonds were obtained in a flow where spanwise mean velocity showed variations as large as 1.3 m/s. This flow field was produced when a slot was

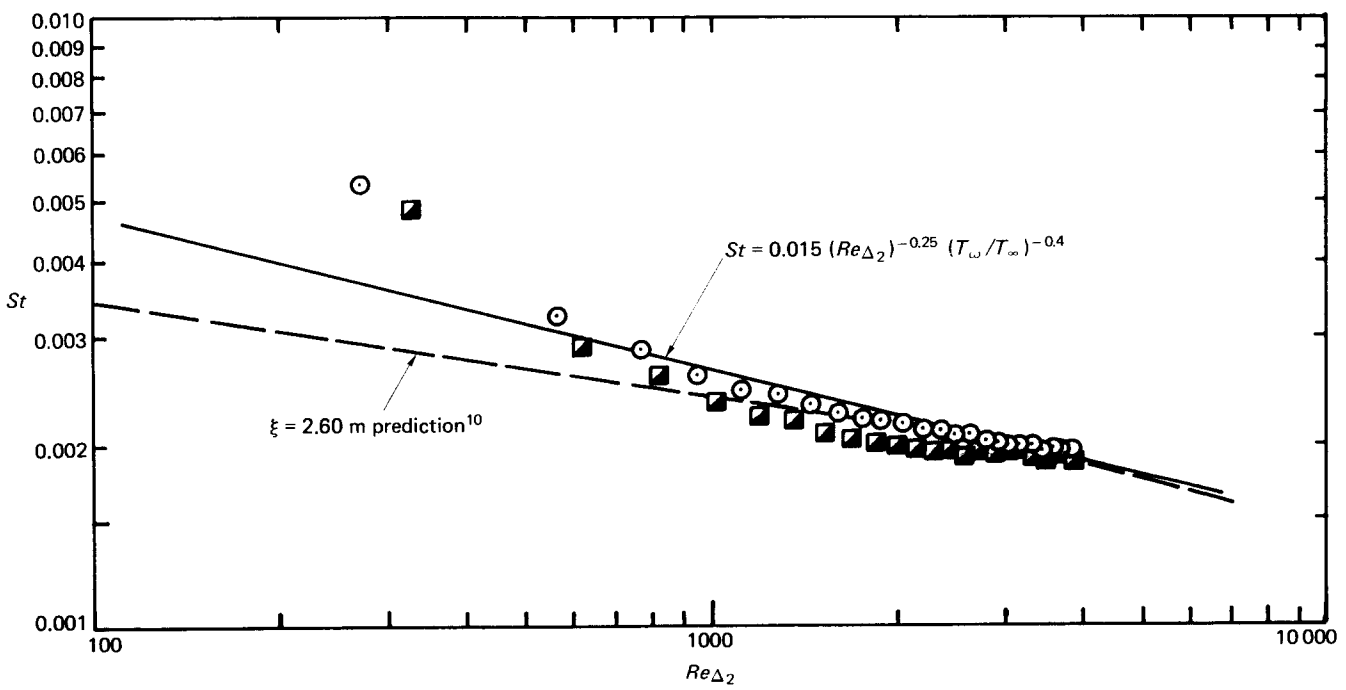

Fig 4 Effects of spire shape changes on Stanton numbers. Symbols given in Table 1

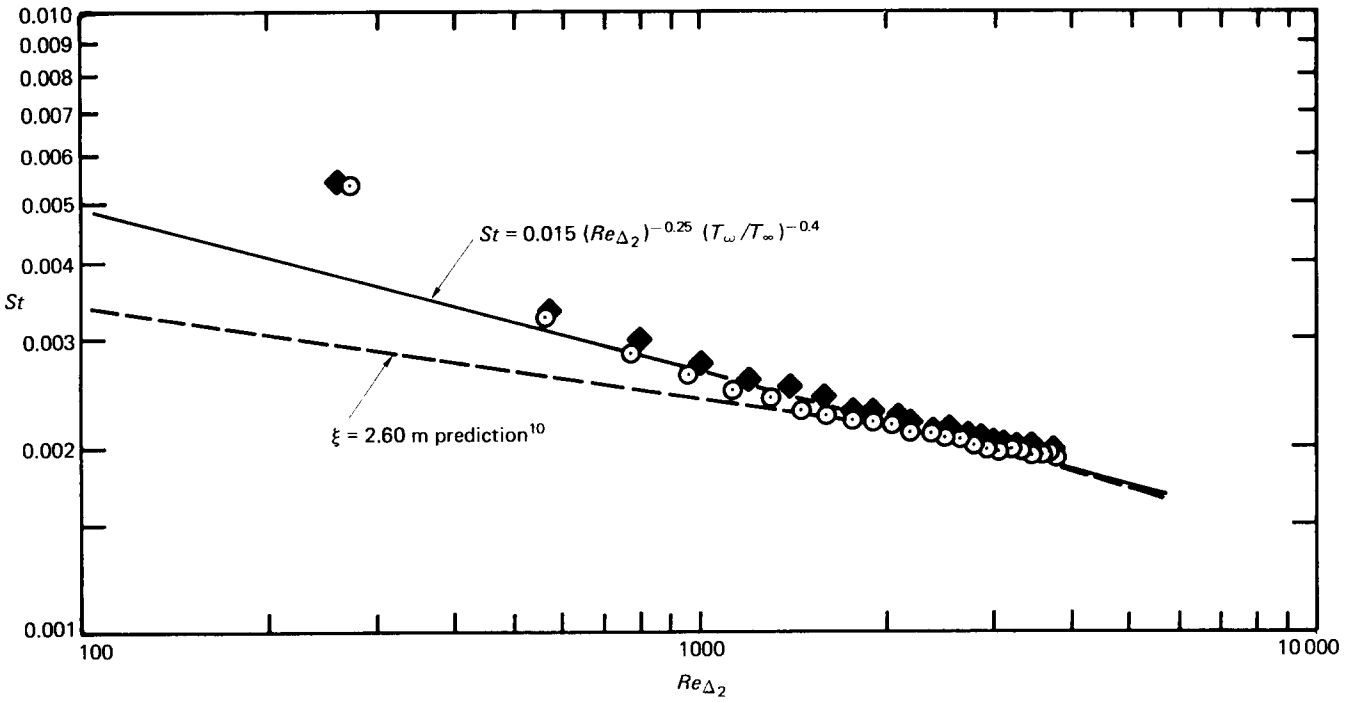

Fig 5 Effects of spanwise mean velocity variations on Stanton numbers. Symbols given in Table 1

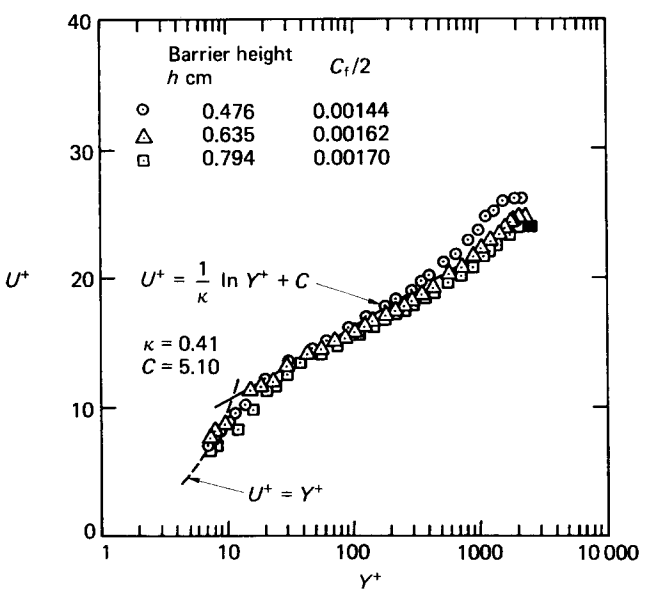

Fig 6 Effect of barrier height h *on mean velocity profiles over the smooth wall,* $x_1 = 1.57$ *m (all profiles with Design C spires). Symbols given in Table 1*

located in the wall upstream of the thickening device to give significant cross-flow velocities which otherwise were not present. Without the slot, and employing the apparatus shown in Fig 1, spanwise velocity varitions were no greater than ± 0.08 m/s across the middle 0.38 m of the tunnel. Fig 5 indicates that differences are small between Stanton numbers with and without time-averaged three-dimensionality. This is partially because each Stanton number point represents a spatial average on the test surface over a 0.50 m spanwise distance and a 0.10 m downstream distance.

Without a slot upstream of the spire array, the level of spanwise uniformity in the flow field depends on the degree of similarity of different spires, and the symmetry of each spire about its vertical axis. If one or more spires are different, then the time-averaged flow field downstream will be three-dimensional. Spatial non-uniformities in the flow seem to coalesce and become spread over larger spatial extents with larger velocity deviations as shear layers convect downstream. Such non-uniformities develop more rapidly as local mean velocities increase.

The development of structural self-similar properties is also a task which increases in difficulty as higher freestream velocities are employed. This is particularly true in regard to the wake, which is strongly dependent on upstream history effects and responds slowly to wall boundary conditions. Here, the lifetime of the largest eddies is approximately $30\delta/U_\infty$, which is equivalent to a downstream distance[12] of 30δ.

Effects of inner region structural adjustments

The inner 10 to 20 percent of boundary layers on smooth surfaces consists of the viscous sublayer, buffer layer, and regions where the mean velocity shows a logarithmic dependence on distance from the wall.

Inner regions may be altered primarily by changing the barrier, especially height h shown in Fig 1. This is evident from the results given in Fig 6 for Design C spires, which show how the relation between the skin friction and mean velocity profiles can be adjusted. In U^+ versus y^+ coordinates, mean velocity data shift downwards and to the right as $C_f/2$ increases with barrier height. In this way, the relationship is changed between the skin friction determined from the shear stress and the skin friction determined from a 'Clauser plot'[13]. Barrier height adjustments also affect the outer region by changing the relation between the skin friction and mean velocity such that the dependence of the Clauser shape factor [13,14]G on downstream distance is altered. G will

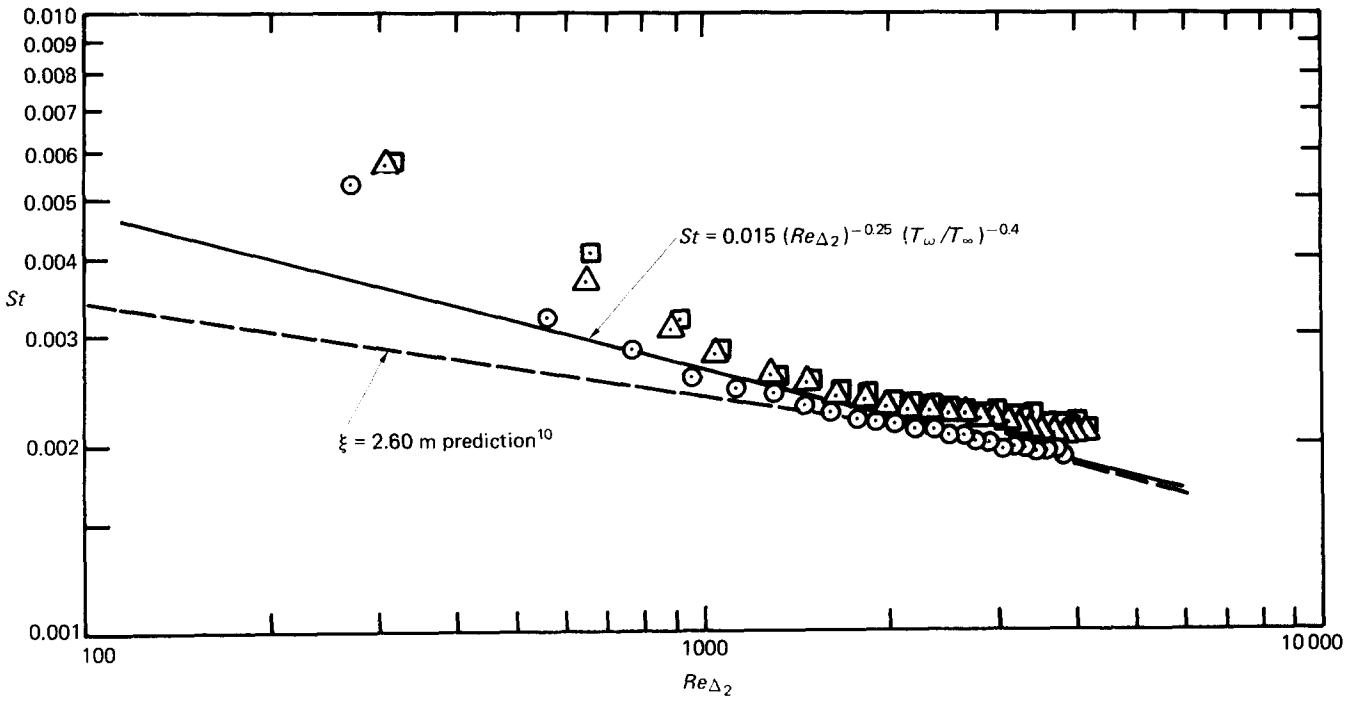

Fig 7 Effect of barrier height changes on Stanton number. Symbols given in Table 1

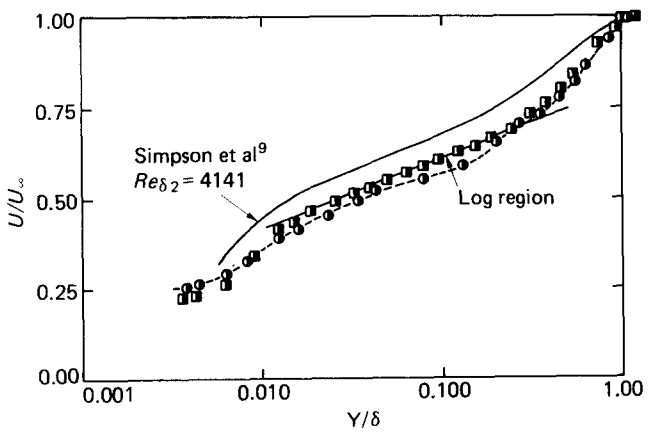

Fig 8 Mean velocity profiles downstream of Design A spires with and without a 0.476 cm barrier. Symbols given in Table 1

increase or decrease with downstream distance, depending on whether the U^+ versus y^+ plots are above or below the law of the wall:

$$U^+ = \frac{1}{\kappa} \ln y^+ + C \tag{4}$$

where $\kappa = 0.41$ and $C = 5.10$. Thus, changing the barrier height is a means by which the flow field can be adjusted to have a low-order type of equilibrium, achieved when G is an invariant with downstream distance and the inner regions of the boundary layer agree with the law of the wall. This occurs when the barrier height h is 0.476 cm for Fig 1 spire geometry.

The variation of Stanton number as inner region structure is changed is shown in Fig 7. At a given enthalpy thickness Reynolds number, a comparison of the three data sets shows that Stanton number increases as the log-regions of mean velocity profiles shift below Eq (4). This behaviour is consistent with the Reynolds analogy and trends shown by skin friction coefficients. According to Refs 15–17, the accepted value of $2St/C_f$ is 1.2 in a fully mature turbulent flow. Results in Figs 6 and 7 deviate from this value by about 14 percent.

Results in Figs 8 and 9 were obtained used Design A spires both with and without a barrier. When no barrier is employed, mean velocity data do not show logarithmic dependence on y at locations where a log-region would nominally be expected. Stanton numbers for these two cases differ slightly at enthalpy thickness Reynolds numbers less than 2000.

Experimental results for rough wall

Results given below show how wall heat transfer and wall shear stress are altered as structural changes are made in a boundary layer developing over a wall consisting of uniform speres roughness. A summary of development steps leading to the flow described in Ref 4 is given in Table 2. All results were obtained at a freestream velocity of 26.8 m/s.

Design C—smooth-wall device

The first trail in the design of the rough-wall thickening apparatus was the smooth-wall design shown in Fig 1. If the Fig 1 device is placed upstream of the rough surface, the resulting flow field has $\overline{u'^2}$ profiles shown in Fig 10. The outer 70 percent of these normalized profiles changes as the layer develops downstream, whereas the inner 30 percent shows some uniformity with downstream distance. The layer is not self-preserving[18], which according to Gartshore and de Croos[19], 'describes a turbulent shear flow whose turbulence is in exact dynamic equilibrium so that the mean distribution of turbulence, non-dimensionalized by a single velocity and length scale, does not change at all in the streamwise direction.' The normalized $\overline{u'^2}$ profiles are also lower than the profile

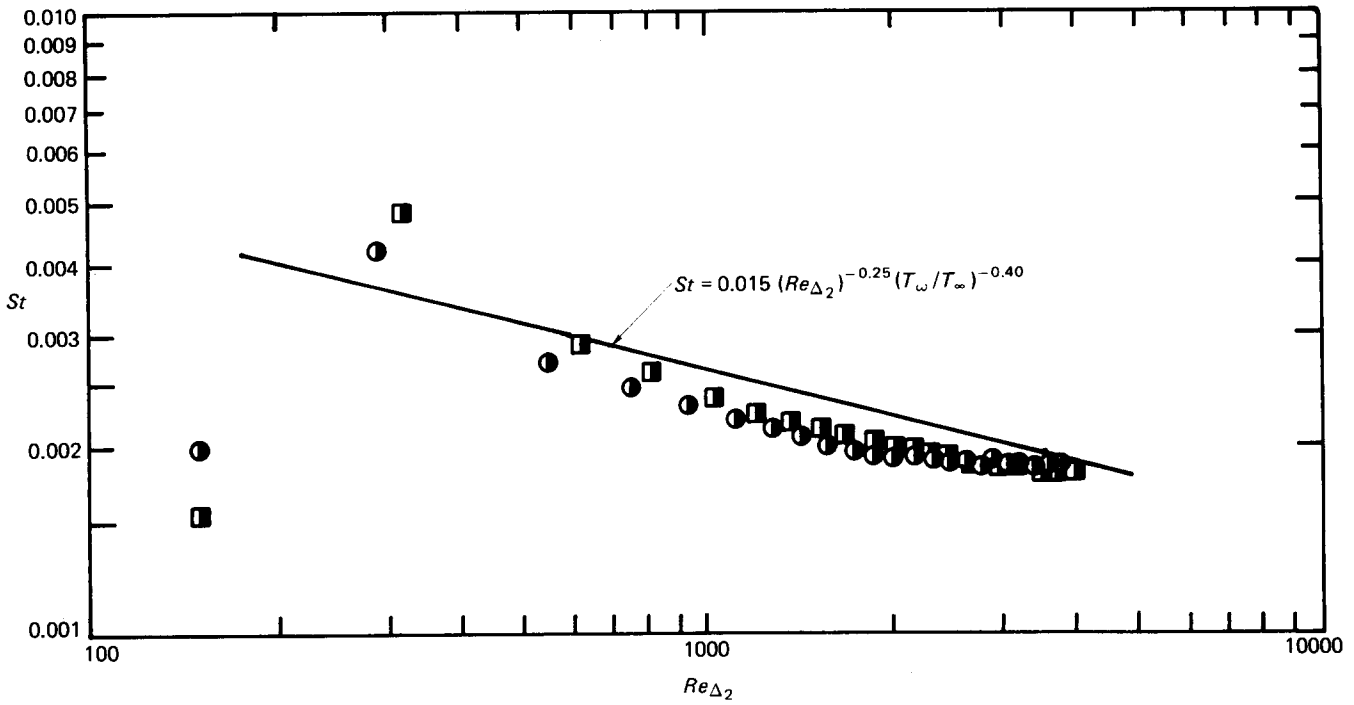

Fig 9 Stanton numbers downstream of Design A spires with and without a 0.476 cm barrier. Symbols given in Table 1

Table 2 Summary of rough-wall test results

Development step	Symbol	Design designation	Design description	Shear layer alteration
1	⊙	C	Smooth-wall design	
2	△	D	Design C with 0.24 cm bar and 0.56 cm barrier	Bar alters the turbulence structure from that given by design C
3	●	E[a]	Design D with 0.64 cm barrier	Barrier height adjustments change the relation between mean velocity and the skin friction coefficient

[a] Produces flow representative of a naturally developing, two-dimensional, flat plate turbulent boundary layer on a rough surface[4]

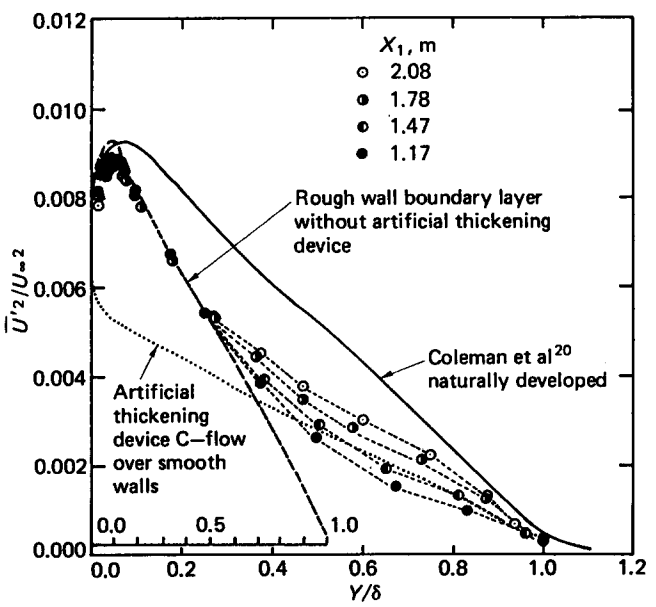

Fig 10 Longitudinal turbulence intensity profiles on the rough surface downstream of Design C thickening device

measured by Coleman[20] in a naturally developing flow over the same test surface.

The $\overline{u'^2}$ profiles seem to result from the superposition of two different turbulence fields: (1) one produced by the naturally developing boundary layer, and (2) one generated from the wakes from the artificial thickening device. The two fields are evident on Fig 10, where (1) extends over about half the y/δ compared with the artificially thickened profile. On this plot, the profile which would result from (1) *only* is denoted by a heavy dashed line. With the addition of (2), $\overline{u'^2}$ magnitudes are increased at locations outside of the naturally developing layer, becoming larger with downstream distance as a result of diffusion of energy from regions closer to the wall. The $\overline{u'^2}$ profile resulting from (2) *only* is indicated by a dotted line and equivalent to that from a smooth-wall flow.

Eventually, if allowed sufficient downstream development, the two turbulence fields would merge together to form an extension of the region influenced by the wall and eventually attain a self-preserving state. However, the mixing from the Design C thickening device

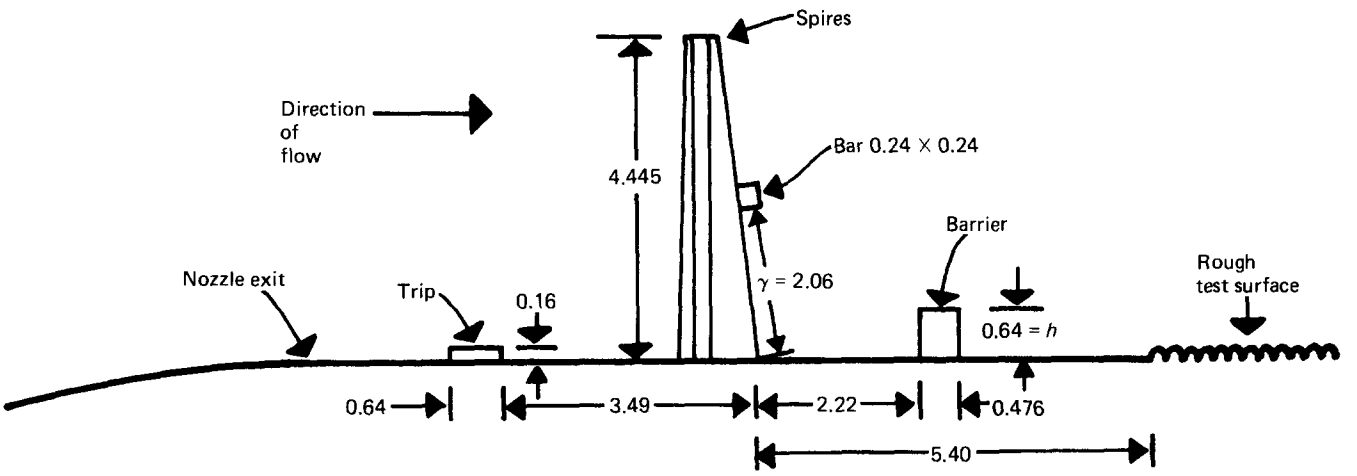

Fig 11 Schematic of Design E rough-wall artificial thickening apparatus. All dimensions: cm

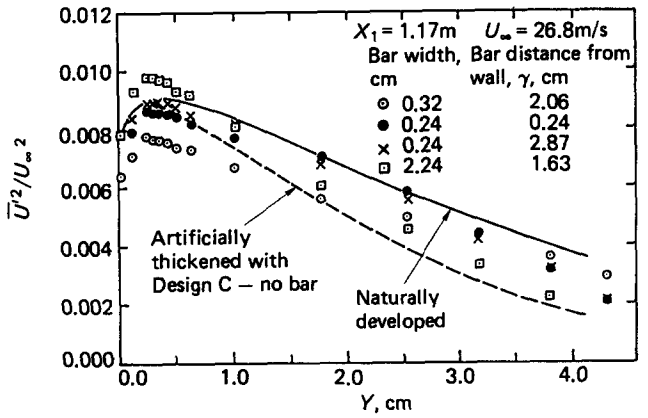

Fig 12 Effect of bar distance from wall, γ, on longitudinal turbulence intensity in artificially thickened rough-wall layers

is not strong enough to accomplish this or to promote sufficient communication between eddies of different size over the rough surface after only 2.4 m of development.

In addition to the lack of self-preservation, the flow from Design C was three-dimensional: (1) the mean velocity field showed spanwise non-uniformities, and (2) magnitudes of the three-dimensional Reynolds stress components, $\overline{u'w}$ and $\overline{v'w'}$ were as large as 40 percent of $-\overline{u'v'}$. Such three-dimensionality was not observed in the smooth-wall tests with a different, but geometrically similar, thickening device.

Design D

The next iterations in apparatus development began with design modifications to achieve a two-dimensional flow field and to modify the turbulence structure. Details of the thickening apparatus were altered, along with several major changes: (1) a square bar having a width of 0.238 cm was added on the downstream side of the spines a distance 2.064 cm away from the wall; (2) the barrier height was changed to 0.56 cm; and (3) the trip was located 3.49 cm upstream of the spires, and its thickness was increased to 0.16 cm. The final geometry for Design D is shown in Fig 11, except here the barrier height is 0.64 cm (Design E).

The final shape and location of the bar were determined after experimentation with a variety of bar shapes and locations. Results from some of these tests are given in Fig 12. These show that significant changes in profiles of $\overline{u'^2}$ result as the distance of the bar from the wall, γ, is altered. As γ increases, magnitudes of $\overline{u'^2}$ in the outer regions of the profile increase and the magnitudes of $\overline{u'^2}$ in the inner regions of the profile decrease. Such quantitative management of turbulence had little or no effect on normalized mean velocity profiles other than slight increases in total boundary layer thickness.

Normalized turbulence profiles from Design D were not self-preserving. In addition, the measured skin friction was different from that required to match log-regions of mean velocity profiles to the equation for fully rough flow conditions:

$$U^+ = \frac{1}{\kappa} \ln\left(\frac{y' + \Delta y}{k_s}\right) + 8.5 \qquad (5)$$

where $\Delta y = 0.023$ cm and $k_s = 0.079$ cm.

Design E—final design

In order to modify the flow so that log-regions of mean velocity profiles matched Eq (5), the barrier height h was changed. As shown in Fig 13, when the barrier height equals 0.56 cm, mean data lie below Eq (5); when the barrier height equals 0.64 cm, mean data show a good match. As for the smooth-wall flow, the relation between the skin friction coefficient and mean velocity could be altered such that G was invariant with downstream distance simultaneously when the near-wall velocities followed the appropriate log-region relation—in this case, given by Eq (5).

Normalized $\overline{u'^2}$ profiles from Designs D and E are compared in Fig 14. In the inner 15 percent of the layers, $\overline{u'^2}$ increases by about 7 percent as barrier height changes from 0.56 cm (Design D) to 0.635 cm (Design E).

Fig 11 shows the final geometry for Design E. With this configuration, normalized profiles of $\overline{u'^2}$ reached a self-preserving state (within measurement uncertainty: ±6 percent) after about 1.6–1.7 m of development. The flow field is described in Ref 4 and has properties similar to a layer which developed naturally on

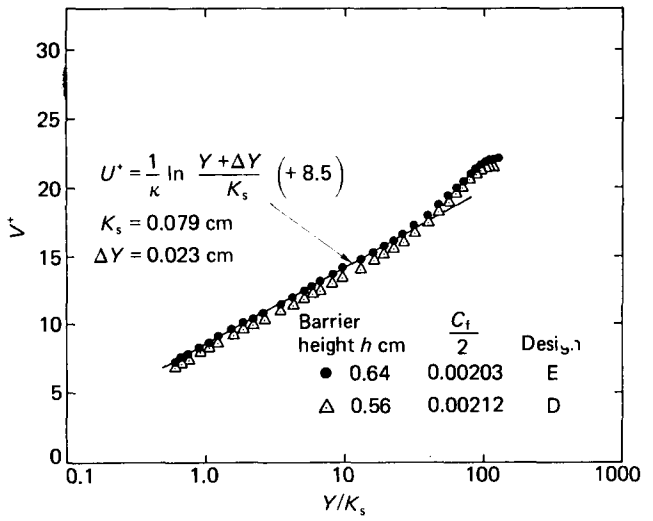

Fig 13 Effect of barrier height h *on mean velocity profiles over the rough wall (all profiles with Design E spires). Symbols given in Table 2*

the same rough surface to the same thickness at the same freestream velocity.

Comparison of flow fields

In Fig 14, turbulence structural characteristics produced by the different rough-wall management devices are compared. These results give evidence of different energy budgets for $\overline{u'^2}$ and turbulence kinetic energy. In many wall-bounded shear layers, production nearly equals dissipation in inner regions, and any imbalance is the result of diffusion by pressure, viscosity or turbulence. Thus, many of the differences between the flows produced by Designs C, D, and E, especially near inner layers, may be tied to diffusion.

Fig 14 shows that the normalized $\overline{u'^2}$ profile from Design D is higher than the one from Design C. This is mostly a result of the bar included with Design D, which promotes communication between eddies in the turbulence field from the thickening device and eddies in the turbulence field from the rough surface. Shear stress distributions downstream of the the Design E configuration are considerably different from the distributions which result downstream of Design C: values of $-\overline{u'v'}/U_\tau^2$ are lower than from Design E, and magnitudes of $\overline{u'w'}/U_\tau^2$ as large as 0.2. These differences are mostly a result of spanwise non-uniformities in flow downstream of Design C, and partially a result of the bar which was included on Designs D and E, and omitted from Design C.

Skin friction coefficients and Stanton numbers measured on the rough wall downstream of the boundary layer management devices are given in Figs 15 and 16. Even though the range of momentum thicknesses in layers produced by Designs C, D, and E vary slightly in the first of these figures, skin friction coefficients are the same within ± 3 percent, a value less than the ± 10 percent uncertainty. Stanton numbers in Fig 16 for Designs C and E are also the same. Thus, attempts to change St and $C_f/2$ by altering the turbulence must result in more significant structural variations than shown in

Fig 14. Levels of wall heat transfer and shear stress are controlled largely by inner region behaviour very near the rough wall. Here, most of the shear stress is due to form drag on roughness elements, and heat transfer rates are limited by thermal resistance from a thin film of fluid covering roughness elements where the only transport mechanism is conduction.

Summary and conclusions

By altering devices used to artificially thicken turbulent boundary layers, shear layers having different turbulence structures were produced. In these flows, the following were managed: (1) mean flow three-dimensionality and

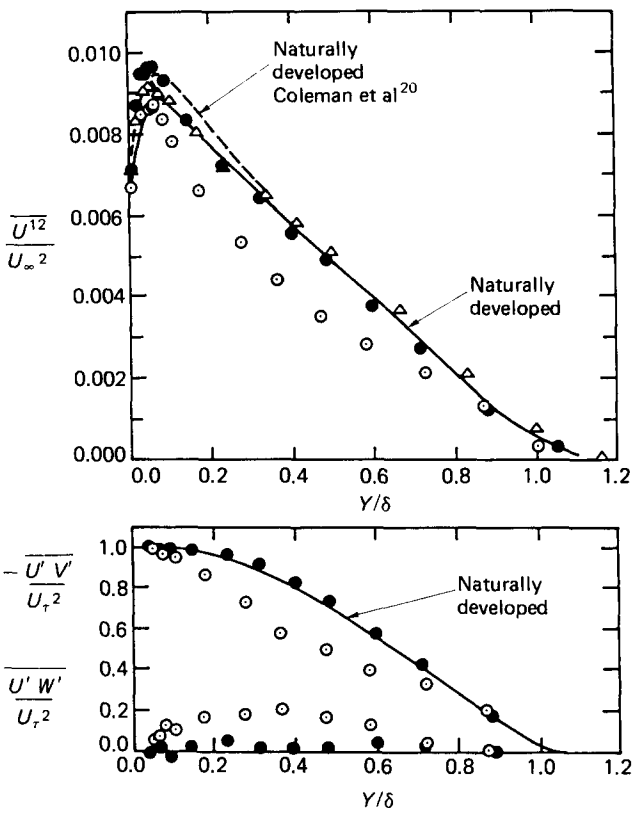

Fig 14 Effect of artificial thickening apparatus geometry changes on turbulence profiles on the rough surface. Symbols given in Table 2

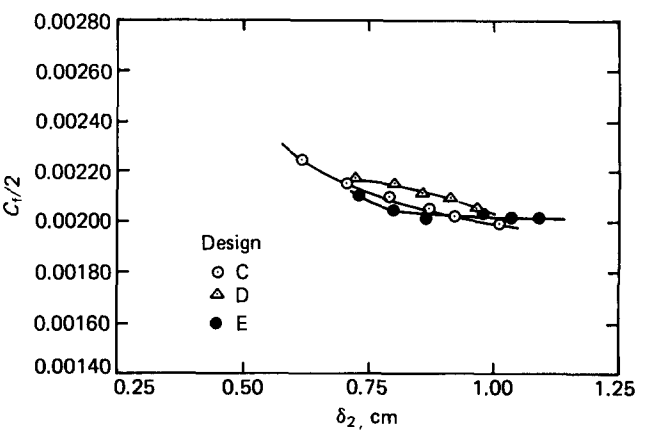

Fig 15 Effects of rough-wall boundary layer management changes on skin friction coefficients. Symbols given in Table 2

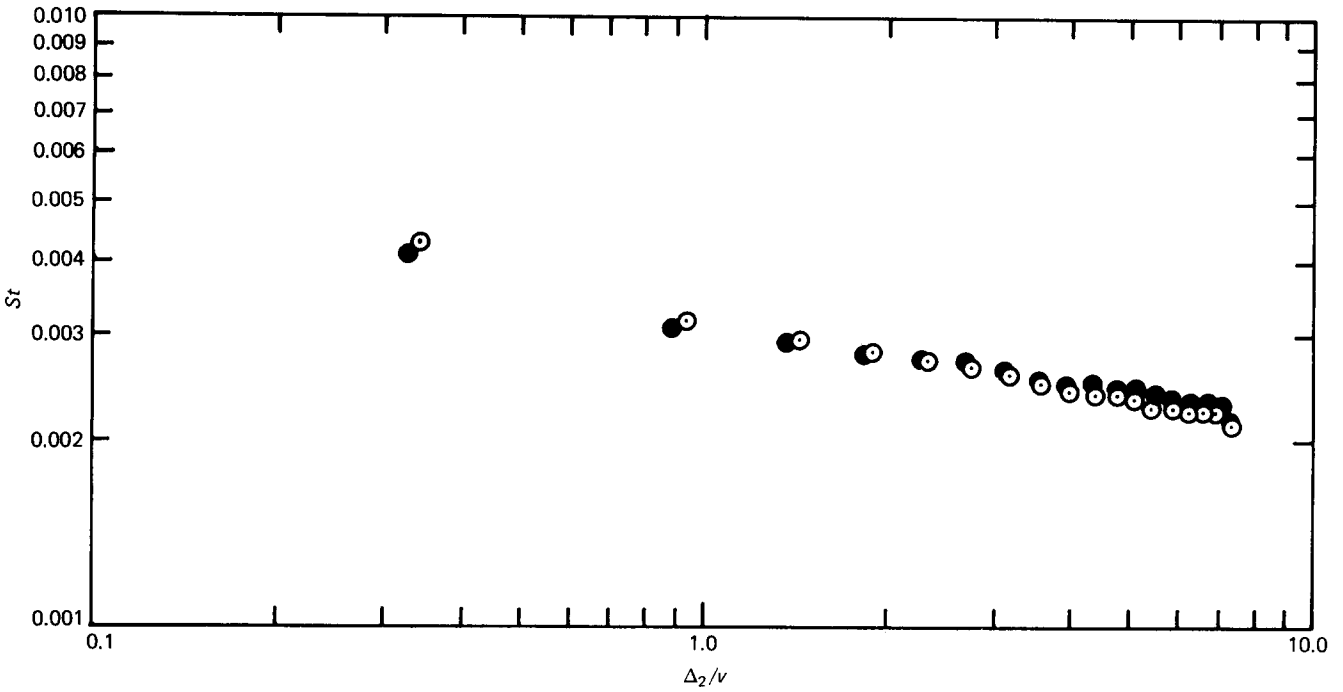

Fig 16 Effects of rough-wall boundary layer management changes on Stanton numbers. Symbols given in Table 2

three-dimensional turbulent shear stresses, (2) the relation between mean velocity in boundary layer log-regions and skin friction coefficients, (3) shapes of mean velocity profiles in outer regions, (4) shapes of mean velocity profiles in inner regions, (5) downstream development of normalized turbulence structure, and (6) on rough surfaces, quantitative levels of shear stress and longitudinal turbulence intensity in inner and outer boundary layer regions independent of mean profile properties.

Of the different types of manipulation studied, the most effective means to alter and control wall heat transfer was alteration of boundary layer regions where mean velocity shows a logarithmic dependence on distance from the wall. This change resulted from one height adjustment of the barrier component of artificial thickening devices. As normalized mean velocity data shifted below the law of the wall, Stanton number increases as large as 29 percent could be produced on smooth surfaces. If mean and turbulence profiles in outer regions of boundary layers were manipulated, Stanton numbers on smooth walls changed by 10 percent or less.

A comparison of the flows over the smooth and rough walls indicated that heat transfer was more easily changed on the former by alterations of turbulence structure. Because of significant form drag and thermal resistance in the flow near roughness elements, structure adjacent to the wall was 'locked' into place and the inner and outer region flow changes produced had little effect on wall heat transfer and wall shear stress.

Acknowledgements

All of the data presented were taken in the Heat Transfer and Turbulence Mechanics Laboratory at Stanford University. The author acknowledges Professor R. J. Moffat's arrangements which made the present study possible.

References

1. **Hunt J. C. R.** Some connections between fluid mechanics and the solving of industrial and environmental fluid-flow problems. *J. Fluid Mech., 1981*, **106**, *103–130*
2. **Bushnell D. M.** Body–turbulence interaction. *AIAA Paper 84-1527, AIAA 17th Fluid Dynamics, Plasmadynamics and Lasers Conference, Snowmass, Colorado, 25–27 June 1984*
3. **Hunt J. C. R. and Fernholtz H. H.** Wind tunnel simulation of the atmospheric boundary layer: a report on Euromech 50. *J. Fluid Mech., 1975*, **70**, *Part 3, 543–559*
4. **Ligrani P. M., Moffat R. J. and Kays W. M.** Artificially thickened turbulent boundary layers for studying heat transfer and skin friction on rough surfaces. *Trans. ASME, J. Fluids Eng., June 1983*, **105**(*2*), *146–153*
5. **Bushnell D. M.** Turbulent drag reduction for external flows, II. *AGARD Report R-723, 1985*
6. **Ligrani P M. and Moffat R. J.** Artificially thickening a smooth-wall turbulent boundary layer. *AIAA J., Aug 1979*, **17**(*8*), *907–910*
7. **Moffat R. J. and Kays W. M.** The turbulent boundary layer on a porous plate: experimental heat transfer with uniform blowing and suction. *Report No. HMT-1, Thermosciences Division, Department of Mechanical Engineering, Stanford University, 1967*
8. **Healzer J. M., Moffat R. J. and Kays W. M.** The turbulent boundary layer on a rough, porous plate: experimental heat transfer with uniform blowing. *Report No. HMT-18, Thermosciences Division, Department of Mechanical Engineering, Stanford University, 1974*
9. **Simpson R. L., Kays W. M. and Moffat R. J.** The turbulent boundary layer on a porous plate: an experimental study of the fluid dynamics with injection and suction. *Report No. HMT-2, Thermosciences Division, Department of Mechanical Engineering, Stanford University, 1967*
10. **Crawford M. E. and Kays W. M.** STAN5—A program for numerical computation of two-dimensional internal and external boundary layer flows. *Report No. HMT-23, Thermosciences Division, Department of Mechanical Engineering, Stanford University, Dec 1975*
11. **Schultz-Grunow F.** New frictional resistance law for smooth plates. *NACA TM 986, 1941*

12. **Bradshaw P.** *An Introduction to Turbulence and its Measurement, The Commonwealth and International Library of Science, Technology, Engineering, and Liberal Studies, Pergamon Press, 1971*

13. **Clauser F. H.** The turbulent boundary layer in *Advances in Applied Mechanics, Academic Press, New York, 1956,* **IV**, *1–51*

14. **Clauser F. H.** Turbulent boundary layers in adverse pressure gradients. *J. Aeronaut. Sci., 1954,* **21**, *91*

15. **Spalding D. B.** Contribution to the theory of heat transfer across a turbulent boundary layer. *Int. J. Heat Mass Transfer, July 1964,* **17**(7), *743–761*

16. **Simonich J. C. and Bradshaw P.** Effect of free-stream turbulence on heat transfer through a turbulent boundary layer. *ASME J. Heat Transfer, Nov 1978,* **100**, *671–677*

17. **Wang T., Simon T. W. and Buddhavarapu J.** Heat transfer and fluid mechanics measurements in transitional boundary layer flows. *ASME Paper No. 85-GT-113, 30th International Gas Turbine Conference and Exhibit, Houston, 18–21 March 1985*

18. **Townsend A. A.** *The Structure of Turbulent Shear Flow, 1st edn, Cambridge University Press, 1956*

19. **Gartshore I. S. and de Croos K. A.** Roughness element geometry required for wind tunnel simulations of the atmospheric wind. *Fluids Engineering Division, ASME Winter Annual Meeting, New York, Dec 1976*

20. **Coleman H. W., Moffat R. J. and Kays W. M.** Momentum and energy transport in the accelerated fully rough turbulent boundary layer. *Report HMT-24, Thermosciences Division, Department of Mechanical Engineering, Stanford University, March 1976*